CHAPTER 8

A New Classification Feature Space and A New Feature Generator

8.1. Introduction

A novel algorithm for rotation invariant texture classification of 3D surfaces using photometric stereo has been proposed in *Chapter 6* and tested in *Chapter 7*. In this chapter, we present improved 3D surface classification strategies to overcome misclassification and achieve higher classification accuracies by introducing a new classification feature space, *radial spectrum*, and a new feature generator, *albedo spectra*.

The structure of this chapter is as follows:

- Both the shortcomings of the classification scheme in *Chapter 6* and the results of misclassification in *Chapter 7* are addressed, and a detailed investigation of the misclassifications is given. We note that there is neither *radial* information nor *albedo* information in our classification scheme described in *Chapter 6*.
- A new classification feature space, *radial spectrum*, is introduced in addition to the polar spectrum.
- In addition, a new feature generator, *albedo spectra*, is presented to provide additional information on surface texture properties.
- In general, the modified surface texture classification scheme is outlined, which combines two main feature spaces:
    1) *polar spectrum* and

2) *radial spectrum*.

We use these feature spaces with two feature generators:

1) *gradient data* and
2) *albedo data*.

- Experimental procedure and results based on our novel photometric stereo texture database are also presented. The comparative study obtained from the different combinations of feature spaces and feature generators is also discussed.
- The final conclusion is drawn.

All test data in this chapter comes from the image set described in *Chapter 7*.

8.2. An Additional Feature Space: Radial Spectrum

In this section, we discuss the misclassification of experimental results described in the previous chapters with the objective of introducing new features to improve the proposed surface rotation invariant texture classification scheme in *Chapter 6*.

8.2.1. Misclassification and Motivation

As we have previously shown in section *7.5.2*, the worst classification performance occurs on the real texture *"rkb1"* and *"bn2"* (*Figure 8. 1a*), with a classification accuracy of *24.07%* and *29.63%* respectively. It is interesting to note that among the testing samples of texture *"rkb1"*, *24* samples out of *54* lead to misclassification of texture *"bn2"*. In another words, nearly *60%* of test samples in the misclassification set (there are *41* test samples in the misclassification set) are misclassified as texture *"bn2"*. Our classification scheme cannot classify these two textures correctly in the majority of the cases.

Figure 8. 1 shows their feature spaces in two ways respectively. We may see that their gradient spectra $M(\omega, \theta)$ are very close in terms of shape and height (the amount of energy in difference at low and high frequency ranges). Their *1D* polar spectra $\Pi(\theta)$, shown in *Figure 8. 1c*, have similar means and furthermore, no obvious peaks. Thus the *SSD* of these two polar spectra is very low.

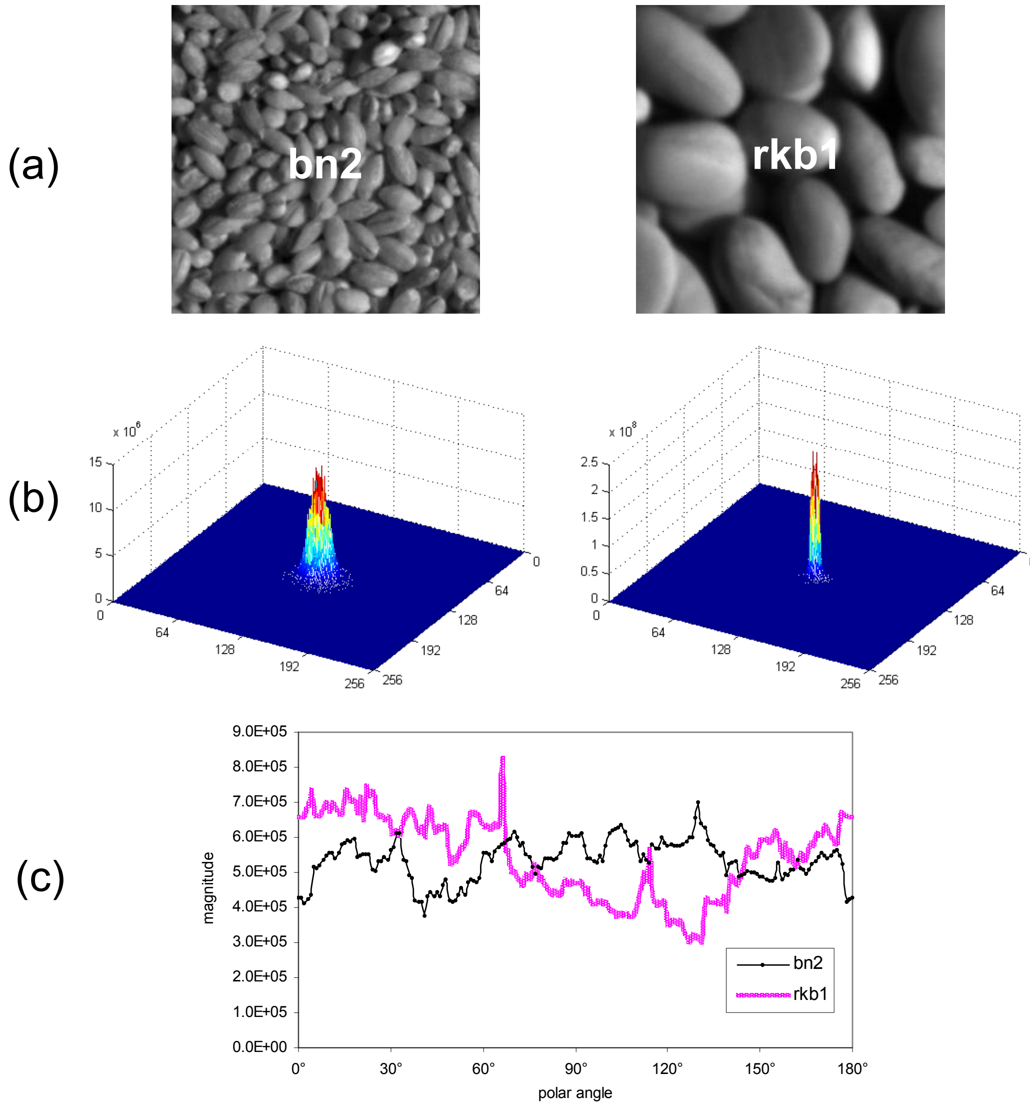

Figure 8. 1 Misclassification between the real texture "bn2" and "rkb1". (a). images of "bn2" and "rkb1"; (b). their gradient spectra $M(\omega, \theta)$; (c). their 1D polar spectrums $\Pi(\theta)$.

Therefore, we may make the conclusion that the polar spectrum *Π(θ)* cannot discriminate between two isotropic textures of the similar variance. In this case, we need an additional feature.

8.2.2. Definition of Radial Spectrum

- ***Definition***

As we saw in *Figure 8. 1b*, even though the frequency distribution of the gradient spectra $M(\omega, \theta)$ are very similar, there are still differences between them especially in the centre of frequency range. Therefore, we introduce a new feature set: the radial spectrum.

The radial spectrum $\Phi(\omega)$ is calculated by integrating of all of the contributions at each radial frequency ω in the image of the gradient spectra $M(\omega, \theta)$:

$$\Phi(\omega) = \int_0^{2\pi} M(\omega, \theta) d\theta \qquad (8.\ 1)$$

We note that this has the advantage that it is *insensitive* to surface rotation in principle. On the other hand, the polar spectrum $\Pi(\theta)$ is *sensitive* to surface rotation, as it sums the magnitudes of all frequencies in one direction θ to produce a measure for the intensity in this direction.

The definition of the radial spectrum is illustrated in *Figure 8. 2* for two of the textures (isotropic texture *"gr2"* and directional texture *"grd1"*). For comparison, we use the same textures for the definition of the polar spectrum. We note that these radial spectra $\Phi(\omega)$ are typical of many textures, having high energy content near the origin and progressively lower values for higher frequencies.

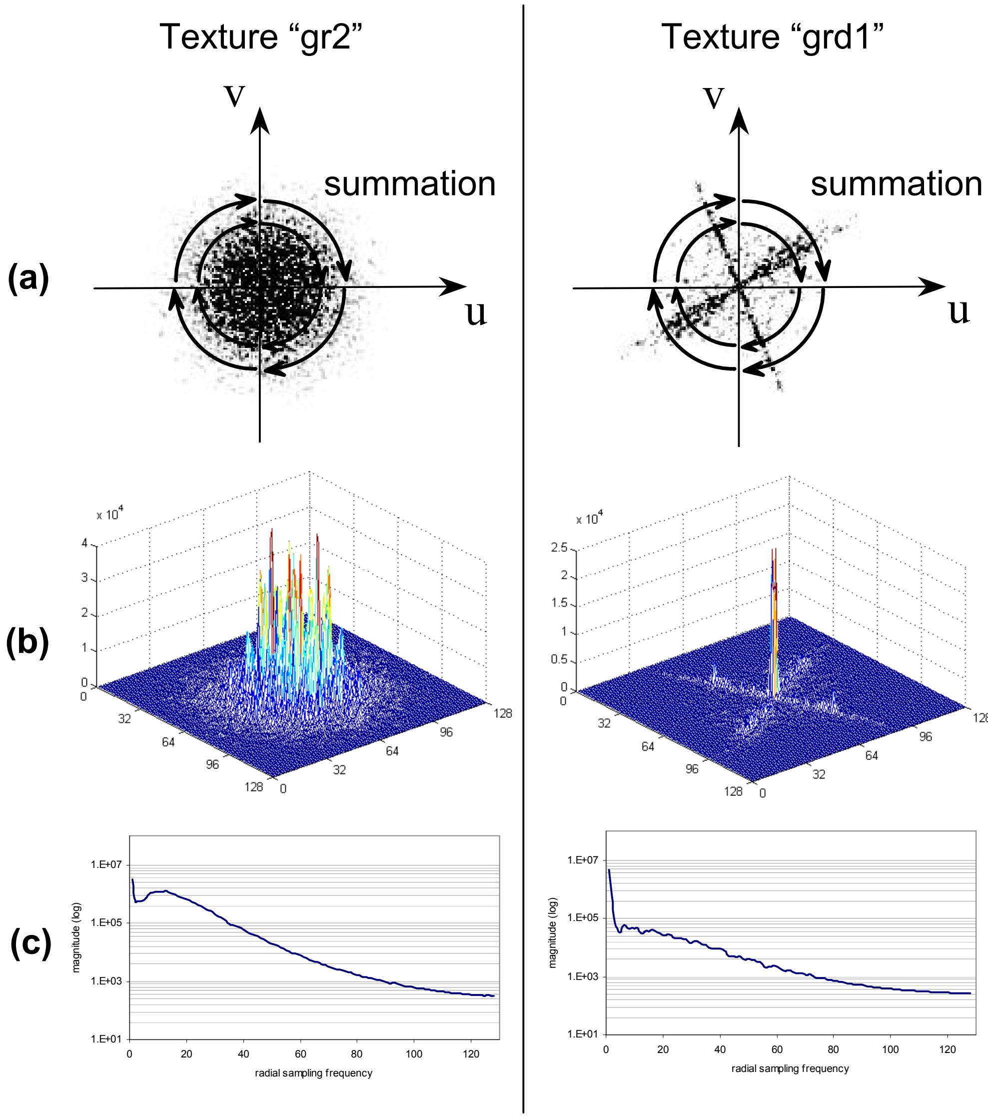

Figure 8. 2 Illustrating the definition of radial spectrum Φ(ω) on gradient spectra M(ω, θ) using two textures gr2 (left column) and grd1 (right column). (a). gGraphical representation of radial spectra on gradient spectra M(ω, θ); (b). M(ω, θ); (c). Radial spectra.

- ***Radial spectra examples***

A selection of four real textures *(gr2, wv2, an4* and *grd1)* is shown in *Figure 8. 3*. Their corresponding radial spectra *Φ(ω)* on gradient spectra *M(ω, θ)* at surface rotation of φ = *30°* are shown in *Figure 8. 4*. These spectra highlight interesting discriminative abilities.

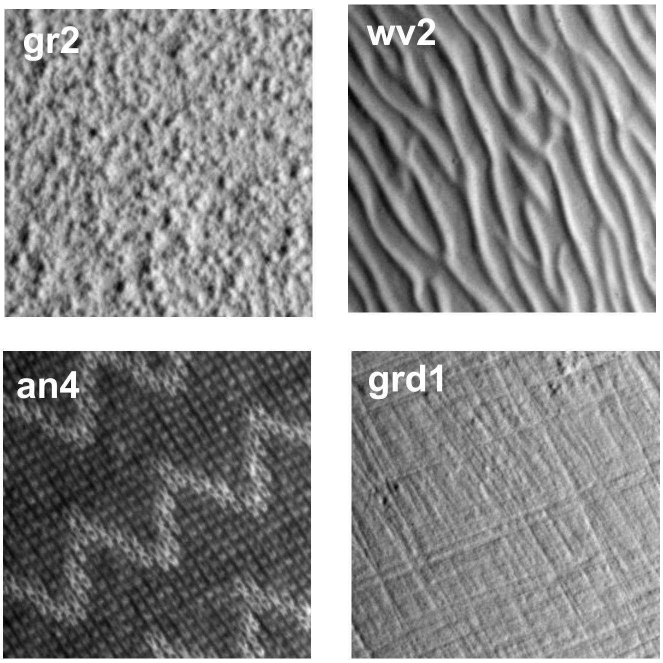

Figure 8. 3 Four real texture samples (gr2, wv2, an4 and grd1) at surface rotation $\varphi = 30°$ with constant illumination tilt angle $\tau = 0°$ and slant angle $\sigma = 50°$.

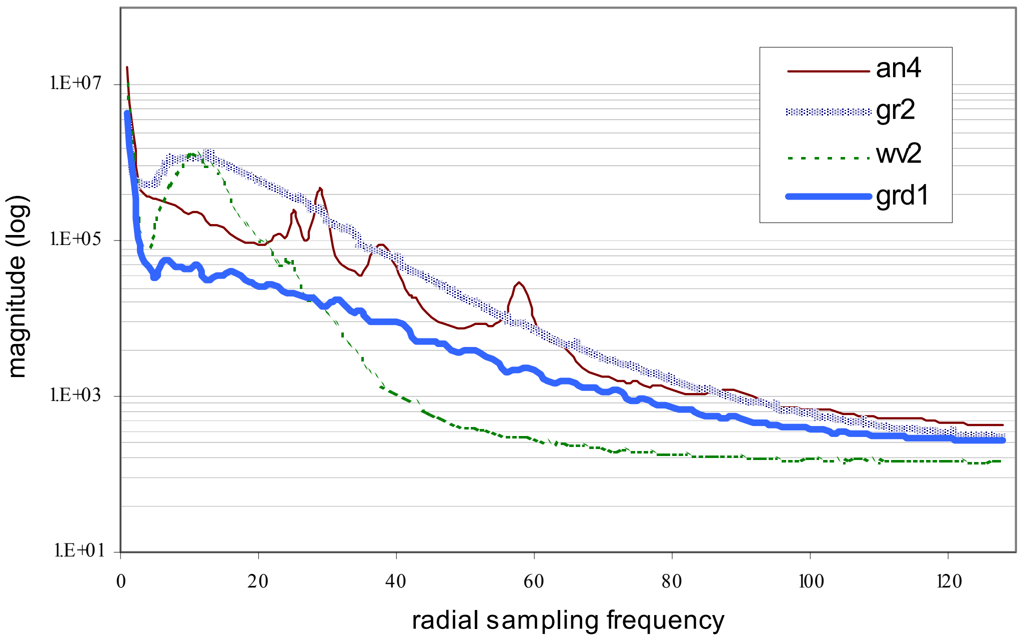

Figure 8. 4 Radial spectra $\Phi(\omega)$ of four selective real textures (gr2, wv2, grd1 and an4) on gradient spectra $M(\omega, \theta)$ at a surface rotation of $\varphi = 30°$.

- ***Expectation of radial spectra of texture "bn2" and "rkb1"***

Regarding the misclassification occurring between textures *"bn2"* and *"rkb1"*, it is interesting to examine the characteristics of their radial spectra *(Figure 8. 5)*. It is obvious that these radial spectra have additional discriminative abilities. Therefore, we expect the classification accuracy for textures *"bn2"* and *"rkb1"* based on the feature space of the radial spectrum $\Phi(\omega)$ to be better than that based on the feature space of the polar spectrum $\Pi(\theta)$ alone.

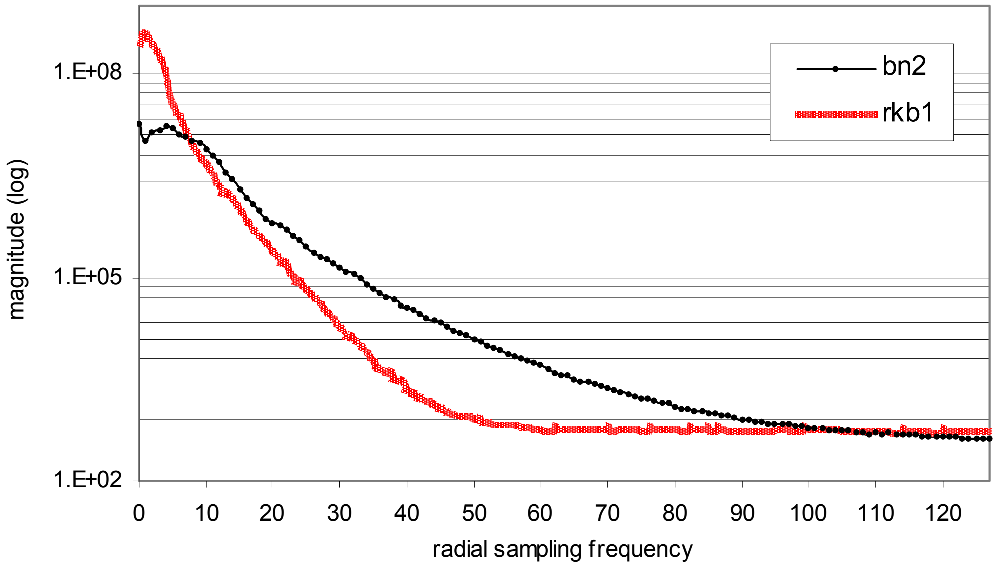

Figure 8. 5 Radial spectra $\Phi(\omega)$ of textures bn2 and rkb1 on gradient spectra $M(\omega, \theta)$ at surface rotation of $\varphi = 0°$.

8.2.3. Examination of Radial Spectrum Insensitivity to Surface Rotation

As the radial spectrum $\Phi(\omega)$ calculates the sum of the magnitude on gradient spectra $M(\omega, \theta)$ in all the directions, the radial spectrum is insensitive to surface rotation. This is shown in *Figure 8. 6*, where the respective radial spectrums $\Phi(\omega)$ of four real textures *(gr2, wv2, grd1 and an4)* at surface rotations of $\varphi = 0°, 30°, 60°, 90°, 120°$ and $150°$ are presented. We note that for each individual texture, there are no obvious differences amongst the radial spectra $\Phi(\omega)$ calculated from those gradient spectra $M(\omega, \theta)$ whatever the surface orientation is.

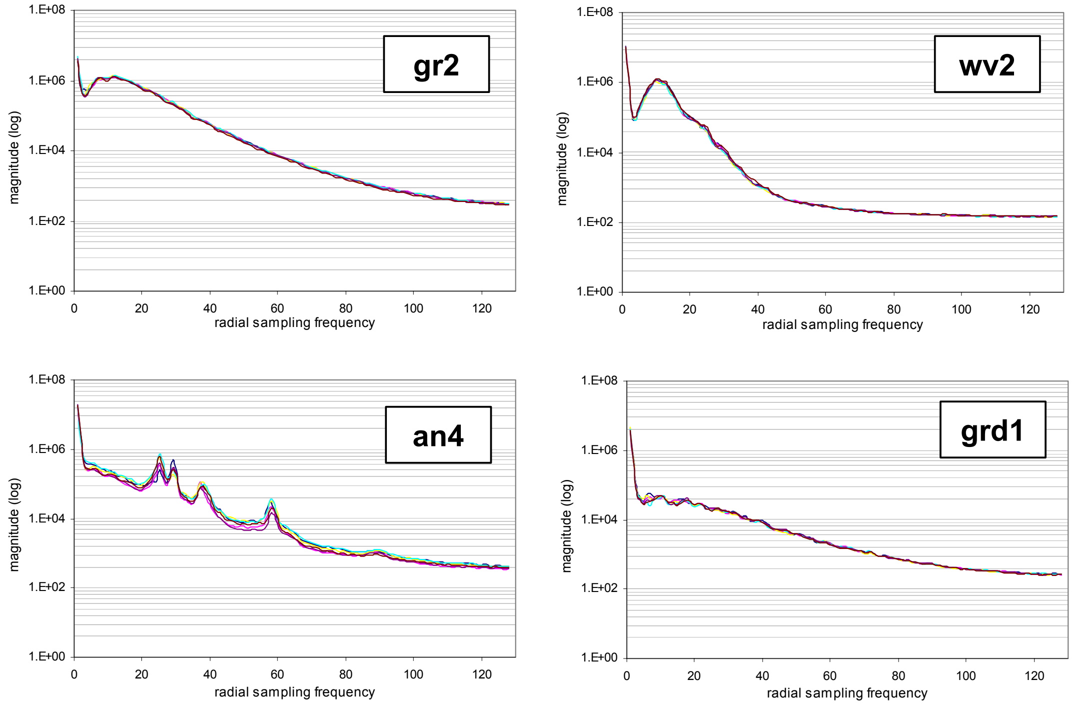

Figure 8. 6 Respective radial spectra $\Phi(\omega)$ of four selective real textures (gr2, wv2, grd1 and an4) on gradient spectra $M(\omega, \theta)$ at surface rotation of $\varphi = 0°, 30°, 60°, 90°, 120°$, and $150°$.

This important property of the radial spectrum allows the comparison of different textures to be performed using a simple sum of squared differences metric and it is not necessary to estimate the surface orientation angle prior to comparison. In other words, comparisons using radial spectra $\Phi(\omega)$ are cheaper computationally than those on polar spectrum $\Pi(\theta)$.

8.2.4. Surface-based Classification Using Radial Spectra Only

- ***Surface-based classification scheme***

The surface-based classification scheme using only the radial spectra $\Phi(\omega)$ on gradient spectra $M(\omega, \theta)$ is summarised in *Figure 8. 7*. This radial spectrum-based classification scheme is quite similar to the polar spectrum-based one illustrated in *Chapter 6* and *Chapter 7.* As the radial spectrum is rotation insensitive, we do not have to estimate the corresponding rotation angle prior to comparison of the sum of squares difference metric between the classes.

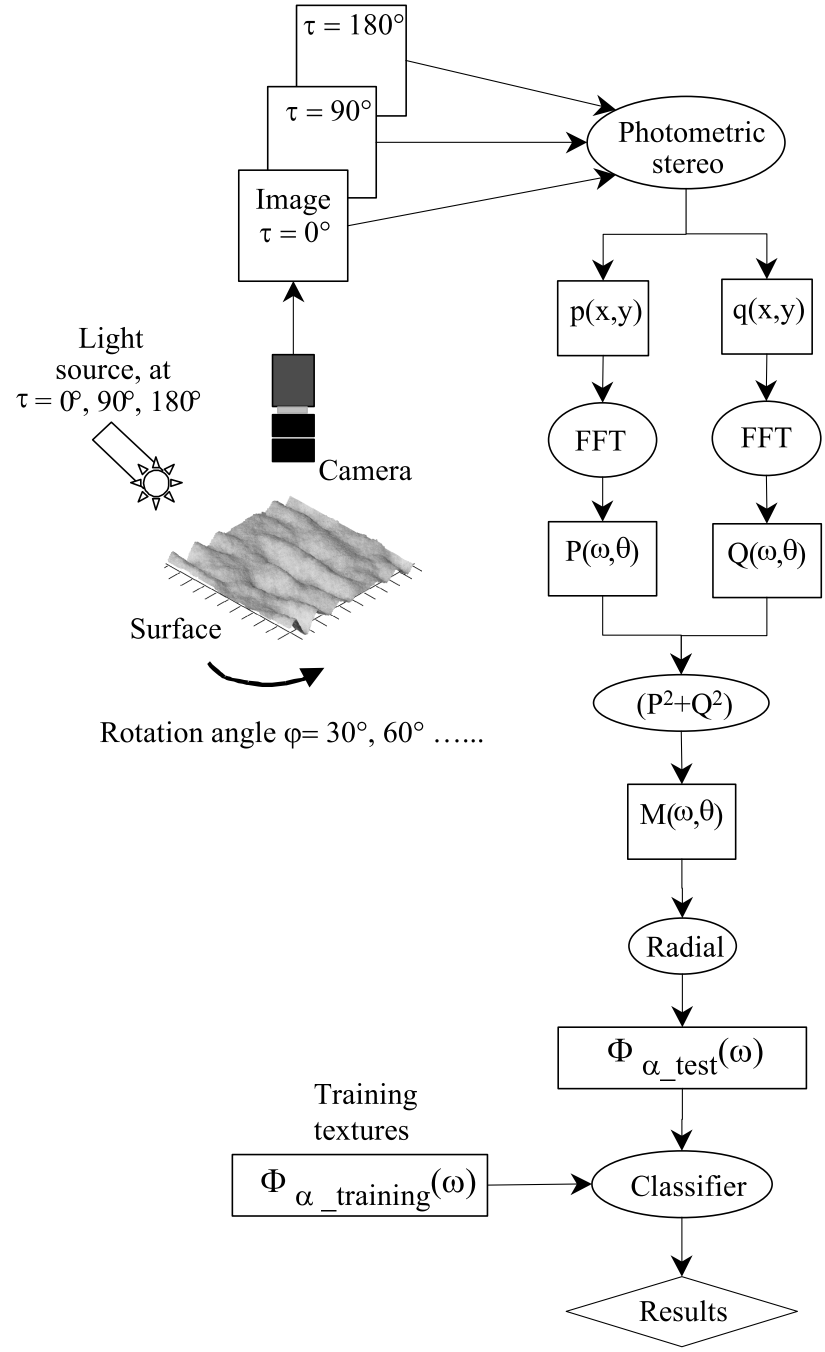

Figure 8. 7 The surface rotation invariant classification scheme using only the feature space of the radial spectrum $\Phi(\omega)$ on gradient spectra $M(\omega, \theta)$.

- ***Presentation of classification results***

Classification results for each real texture class are shown in *Figure 8. 8*. In addition, we also show the classification results (polar-spectrum-based) obtained in *Chapter 7* for comparison.

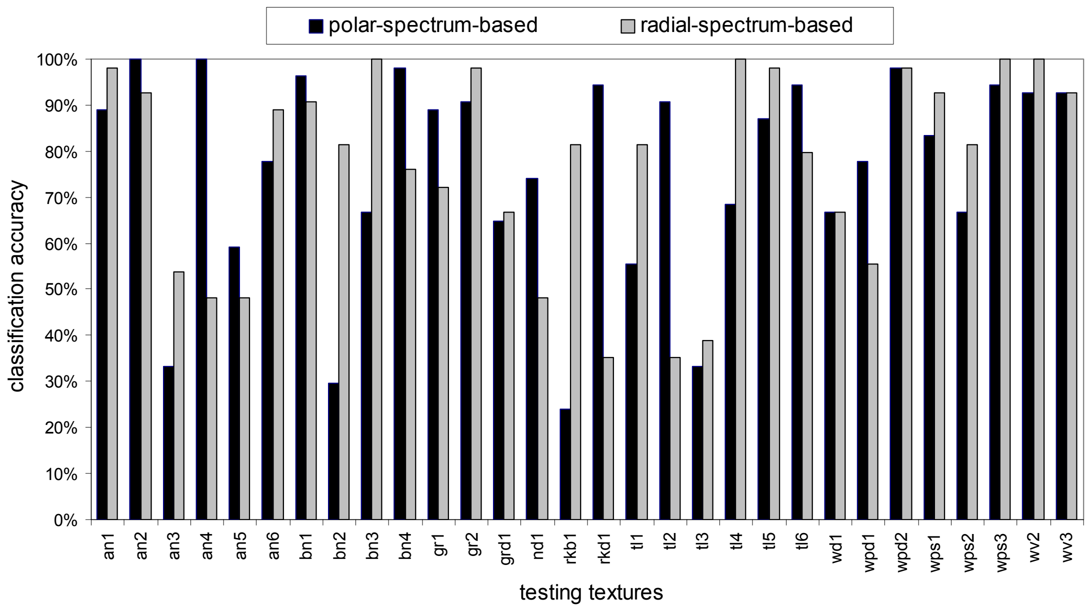

Figure 8. 8 Classification results for 30 real textures for radial spectrum feature space $\Phi(\omega)$ and polar spectrum feature space $\Pi(\theta)$ on gradient spectra $M(\omega, \theta)$.

The radial spectrum classifier achieves an average classification accuracy of *76.7%* for the same thirty real textures as used in the previous experiment in *Chapter 7*. Compared to the average classification accuracy of *76.3%* based on the polar spectrum $\Pi(\theta)$ for the same texture data set, there is little difference between them. However, as we see in *Figure 8. 8*, for some of individual real textures, their correct recognition rate changes dramatically between these two feature spaces.

- ***Discussion of classification results***

It is also interesting to note that as what we have expected, the performance of the "radial spectrum" classifier on texture *"bn2"* and *"rkb1"* is better than that obtained using the "polar spectrum" classifier. For texture *"bn2",* the correct recognition rate increases to *81.48%* from *29.63%*. On the other hand, for texture *"rkb1"* its correct recognition rate increases to *81.48%* from *24.07%.*

Although the classification accuracy of the radial spectrum-based scheme has improved and is better than that of polar spectrum-based scheme (especially for some of the isotropic textures such as *bn2, rkb1, an3,* and *bn3*), some of the directional textures give a worse performance on radial spectrum-based scheme compared to that of polar spectrum-based scheme. Texture *an4, nd1, rkd1* and *wpd1*. The summary of classification accuracy is shown in *Table 8. 1*.

Classification accuracy		Classifier based on gradient spectra $M(\omega, \theta)$	
		Polar-spectrum-based $\Pi(\theta)$	Radial-spectrum-based $\Phi(\omega)$
Overall 30 real textures		**76.30%**	**76.67%**
Isotropic texture samples	*bn2*	29.63%	81.48% ↑
	rkb1	24.07%	81.48% ↑
	an3	33.33%	53.07% ↑
	bn3	66.67%	100.00% ↑
Directional texture samples	*an4*	100.00%	48.15% ↓
	nd1	74.07%	48.15% ↓
	rkd1	94.44%	35.19% ↓
	wpd1	77.78%	55.56% ↓

Table 8. 1 Classification accuracy comparison between the polar spectrum-based scheme and radial spectrum-based scheme on gradient spectra $M(\omega, \theta)$, for 30 real textures.

8.2.5. Image-based Classification Using Radial Spectra Only

In the section, we introduce an image-based classification scheme using radial spectra only (see *Figure 8. 9*), as the comparison to the surface-based classification scheme. This classification is done in a similar way in which we present the image-based classification scheme using polar spectra in Chapter *6*.

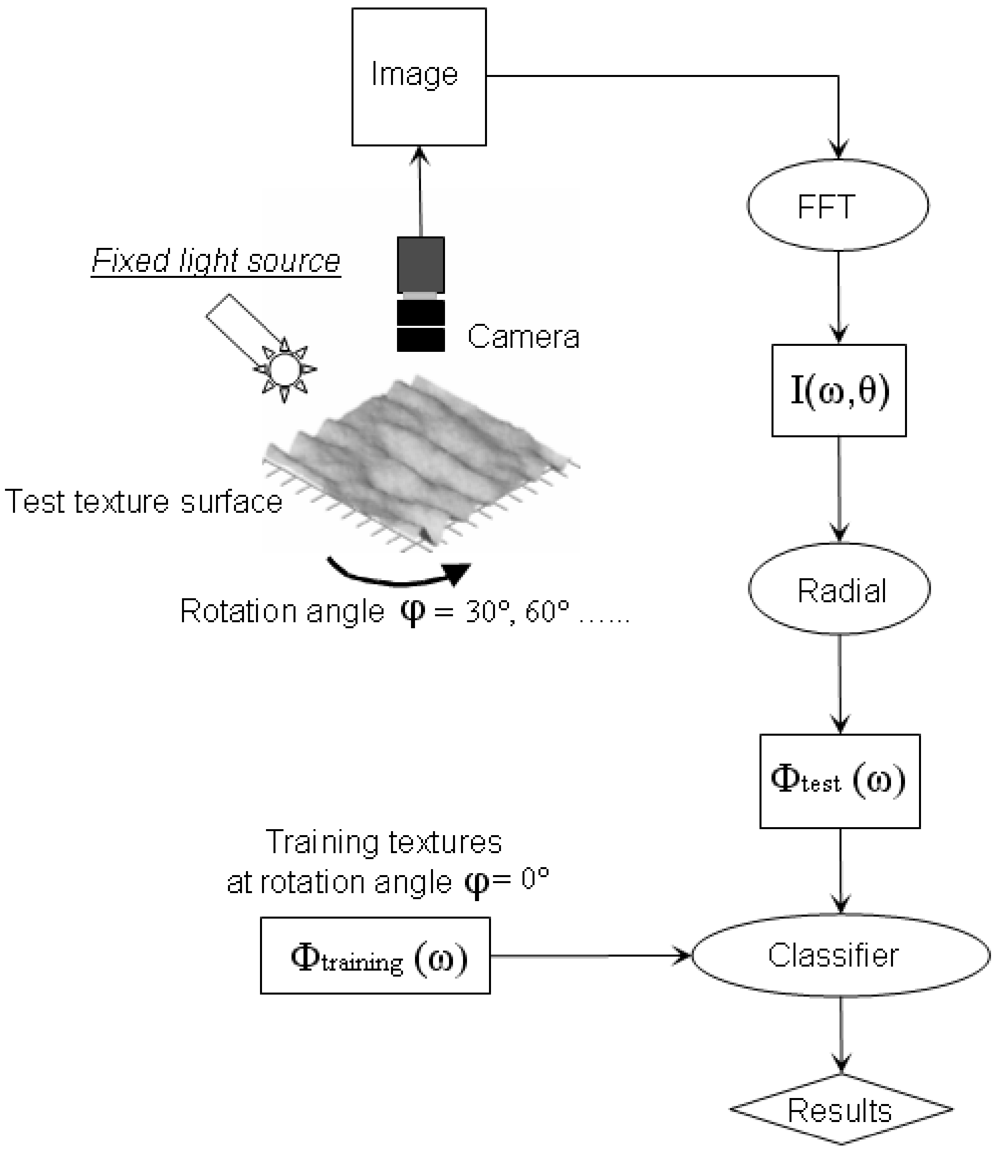

Figure 8. 9 Image-based texture classification scheme using radial spectra only.

The image-based classifier using radial spectrum only achieves an average classification accuracy of *35.3%* (*Figure 8. 10*). Compared to the average classification accuracy of *76.7%* based on the surface information for the same texture data set, it can be understood that this scheme is not surface invariant texture classification scheme. It also proofs that *3D* surface rotation is not the same as *2D* image rotation, while considering the effect of illumination conditions.

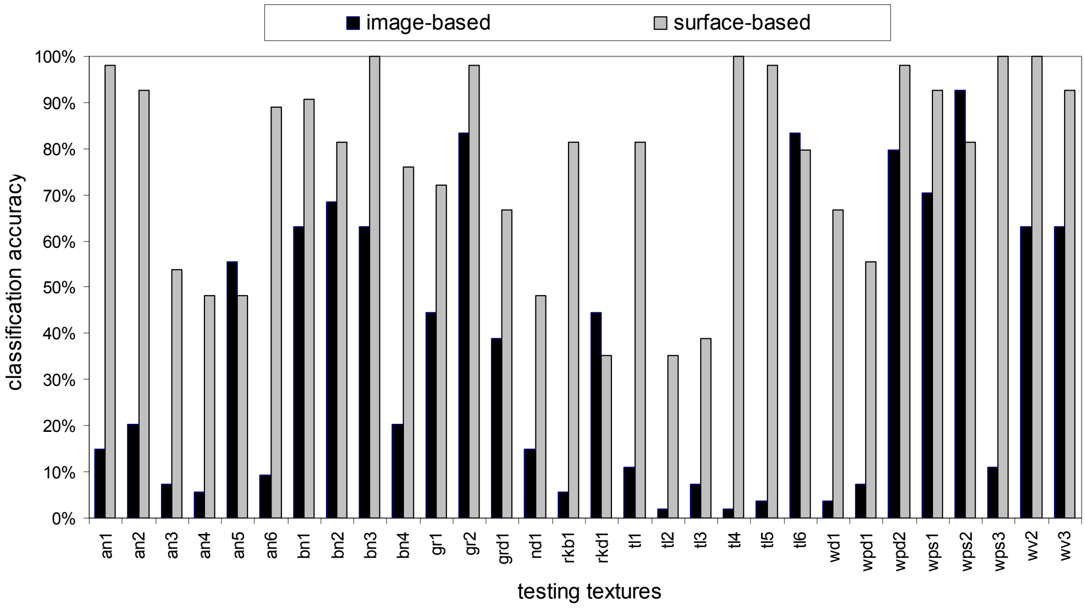

Figure 8. 10 Image-based and surface-based classification results for 30 real textures for radial spectrum feature space $\Phi(\omega)$.

8.3. New Feature Generator: Albedo Spectra

8.3.1. Misclassification and Motivation

Looking back to the classification results in *section 7.5.2*, we note that the texture *"tl3"* classification accuracy of *33.33%* gave the poorest performance. Through deeper investigation, we find that:

- there are *13* samples of *"tl3"* misclassified as *"an2"*;
- there are *23* samples of *"tl3"* misclassified as *"tl5"*,

among *54* test samples. It is easier to understand why the misclassifications take place among textures *"tl3", "an2"* and *"tl5"*. In *Figure 8. 11*, gradient spectra $M(\omega, \theta)$ of real textures *"tl3", "an2"* and *"tl5"* and their polar spectra $\Pi(\theta)$ are shown together. We note that after translating the polar spectrum of texture *"tl3"*, the dominant peaks of all three polar spectra are lying close together except for three small peaks of the polar spectrum of texture *"an2"*. This explains the misclassifications, as the values of the cost function are very close to each other.

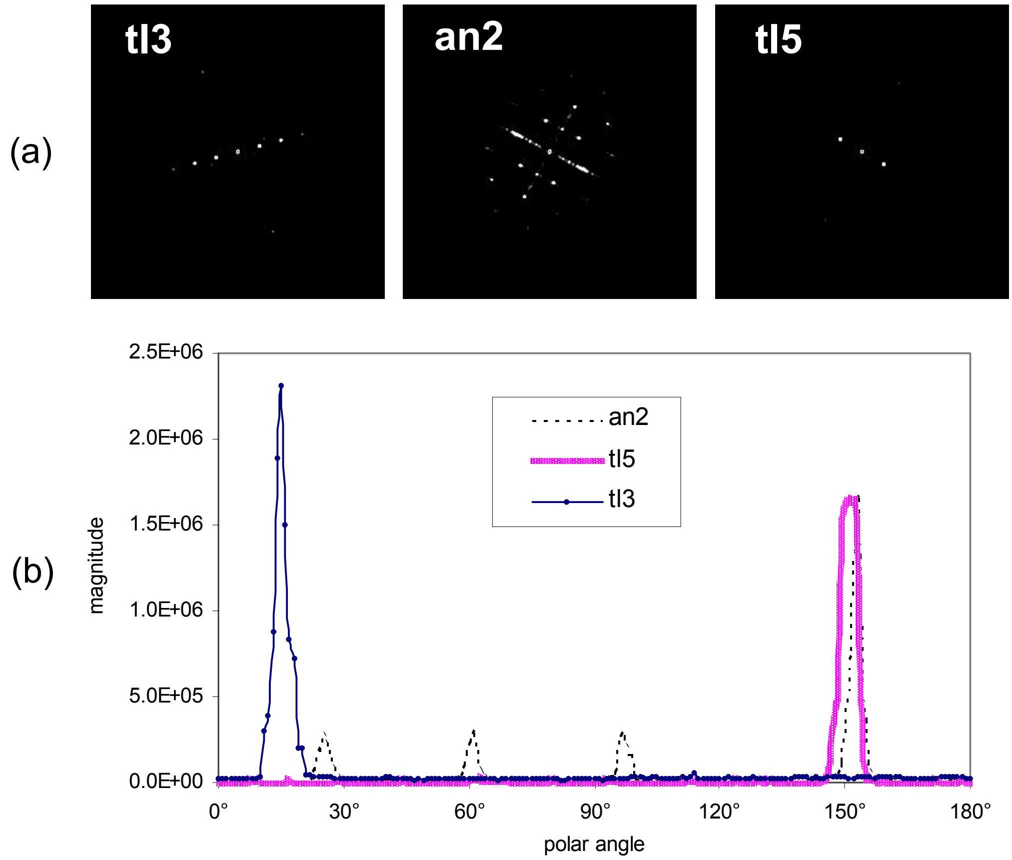

Figure 8. 11   Misclassification which occurred with real texture "tl3". (a). gradient spectra $M(\omega, \theta)$ of real textures "tl3", "an2" and "tl5" respectively; (b). their 1D polar spectrums $\Pi(\theta)$ integrated together.

Examining the original surface images of these three textures in *Figure 8. 12* shows that there are significantly different texture patterns appearing in their surface images. On the other hand their relief images, on which our classifier really depends, are similar to each other. However, these patterns remain in the albedo image and our current classifier discards this information.

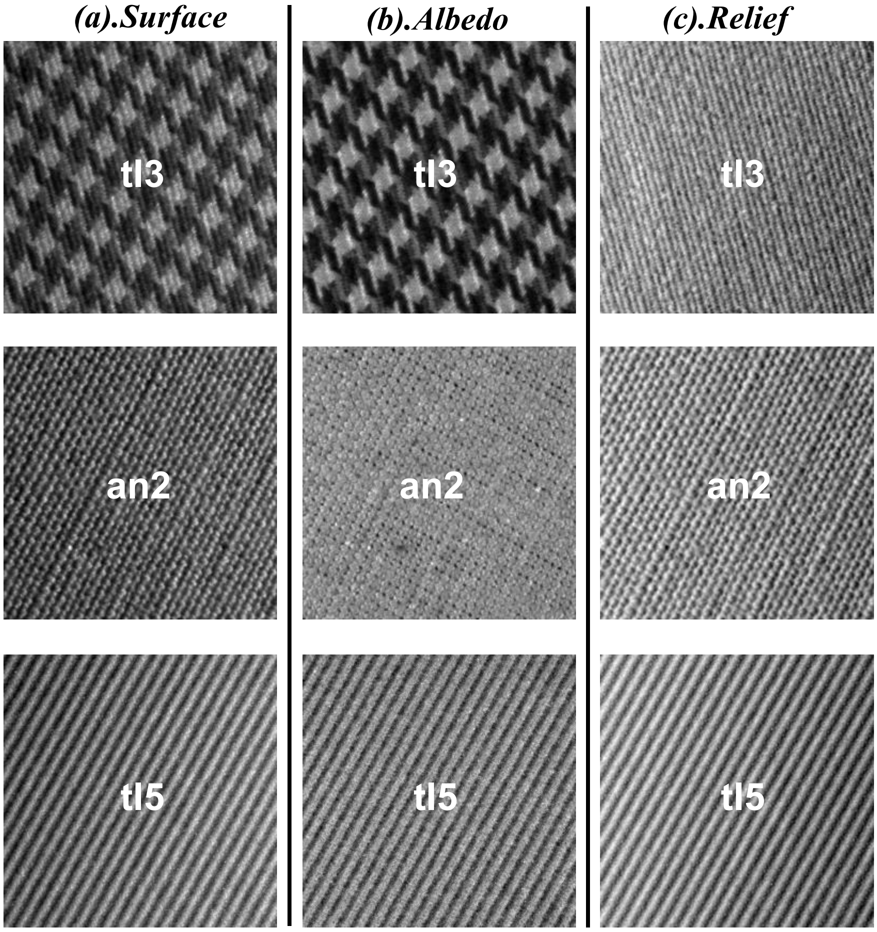

Figure 8. 12 Surface images, albedo images and relief images for real texture "tl3", "an2" and "tl5" respectively.

The conclusion drawn for the investigation of misclassification of texture *"tl3"* is that the albedo information is also important for classification, and cannot be ignored.

8.3.2. New Feature Generator: Albedo

- ***Obtaining albedo images***

From the experiments described in chapter 7, we have already obtained the surface partial derivatives $p(x, y)$ and $q(x, y)$. They can be used at each (x, y) to solve for the albedo data $\rho(x, y)$ [McGunigle98] [Kay95] [Woodham80]. Thus albedo data $\rho(x, y)$ can be easily obtained as below:

$$\rho(x,y)=\frac{i(x,y)}{\left(\frac{-p(x,y)\cos\tau\sin\sigma-q(x,y)\sin\tau\sin\sigma+\cos\sigma}{\sqrt{p^2(x,y)+q^2(x,y)+1}}\right)} \tag{8. 2}$$

where: $\rho(x, y)$ is the albedo of the surface;

σ, τ are the illuminant's slant and tilt angles;

$p(x, y)$ and $q(x, y)$ are surface partial derivatives; and

$i(x, y)$ is image intensity.

- ***Albedo spectra in the frequency domain***

As both the polar spectrum and radial spectrum features are calculated in the frequency domain, the albedo data must be Fourier transformed. The albedo function $\rho(x,y)$ does not suffer from the same directional artefacts as the partial derivatives and may therefore be directly transformed and used:

$$A(\omega,\theta)=\Re\,[\rho(x,y)] \tag{8. 3}$$

where $A(\omega, \theta)$ is the albedo spectra in the frequency domain.

- ***Polar spectra and radial spectra derived from albedo spectra***

The polar spectrum $\Pi_\beta(\theta)$ and radial spectrum $\Phi_\beta(\omega)$ of the albedo data $\rho(x,y)$ are defined below:

(1). $$\Pi_\beta(\theta)=\int_0^\infty A(\omega,\theta)\,d\omega \tag{8. 4}$$

(2). $$\Phi_\beta(\omega)=\int_0^{2\pi} A(\omega,\theta)\,d\theta \tag{8. 5}$$

where ω is radial frequency in polar co-ordination,

θ is the polar frequency angle in polar co-ordination,

$A(\omega, \theta)$ is the albedo spectra in the frequency domain,

$\Pi_{\beta}(\theta)$ is the albedo-based polar spectrum, and

$\Phi_{\beta}(\omega)$ is the albedo-based radial spectrum.

Note that, in order to discriminate between the polar spectra and radial spectra based on gradient spectra $M(\omega, \theta)$ and albedo spectra $A(\omega, \theta)$, we re-define the polar spectrum on gradient data as $\Pi_{\alpha}(\theta)$, and the radial spectrum on gradient data as $\Phi_{\alpha}(\omega)$. This is summarised in *Table 8. 2*.

	Gradient spectra $M(\omega, \theta)$	Albedo spectra $A(\omega, \theta)$
Polar spectrum	$\Pi_{\alpha}(\theta)$	$\Pi_{\beta}(\theta)$
Radial spectrum	$\Phi_{\alpha}(\omega)$	$\Phi_{\beta}(\omega)$

Table 8. 2 Definition of the polar spectrum and radial spectrum on both gradient spectra and albedo spectra.

Recalling the misclassifications that occurred between textures *"tl3", "an2"* and *"tl5"*, we expect that the albedo data should be better than surface relief data in the classifier. *Figure 8. 13* where albedo spectra $A(\omega, \theta)$ plus corresponding polar spectrum $\Pi_{\beta}(\theta)$ and radial spectrum $\Phi_{\beta}(\omega)$ for real textures *"tl3", "an2"* and *"tl5"* are shown respectively, confirms this expectation. We note that both the polar spectra $\Pi_{\beta}(\theta)$ and the radial spectra $\Phi_{\beta}(\omega)$ calculated on albedo data have a discriminative ability compared with those obtained from gradient spectra $M(\omega, \theta)$.

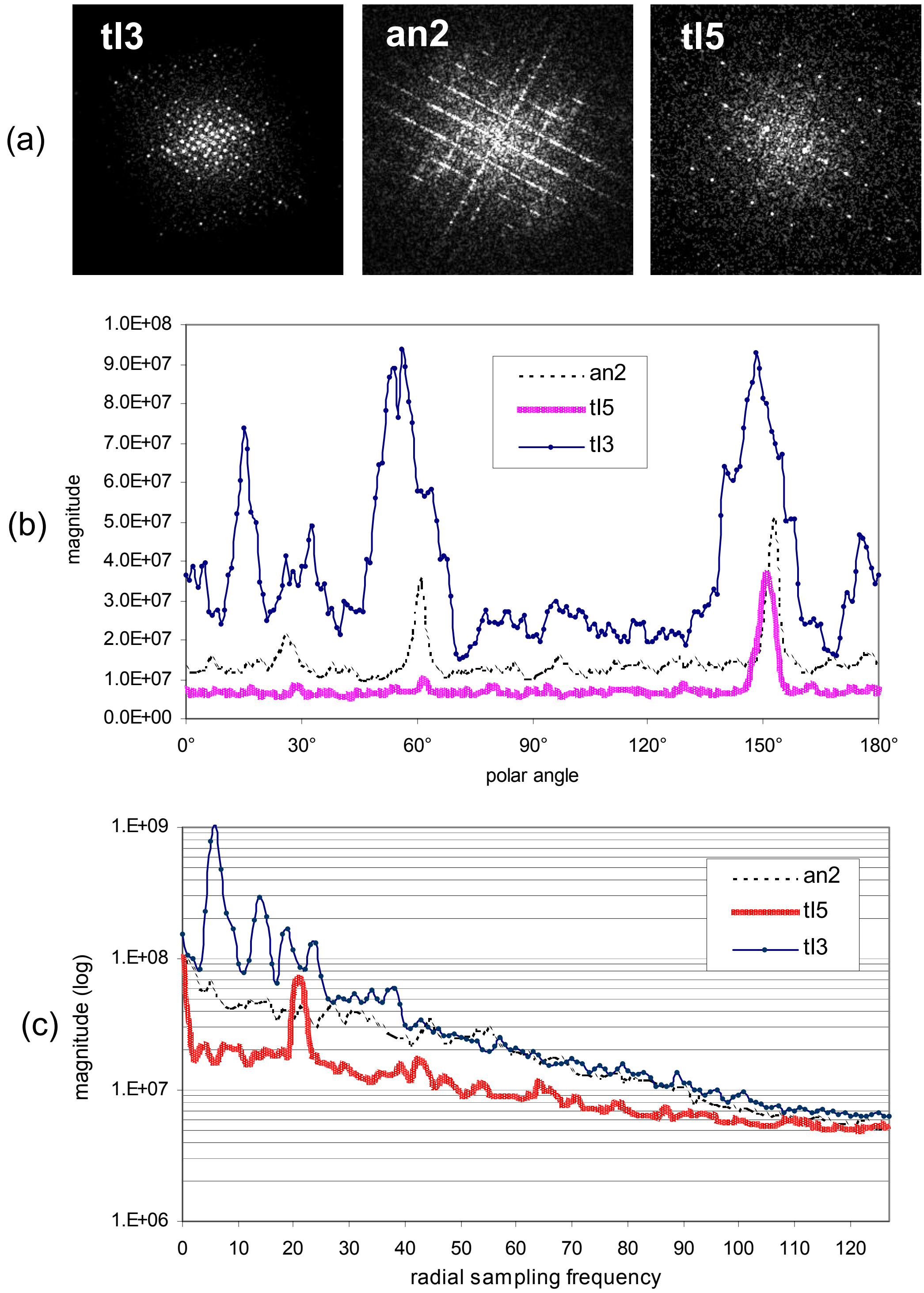

Figure 8. 13 Albedo spectra plus the corresponging polar spectrum and radial spectrum for real texture "tl3", "an2" and "tl5" respectively. (a). albedo spectra $A(\omega, \theta)$. (b). polar spectrum $\Pi_\beta(\theta)$. (c). radial spectrum $\Phi_\beta(\omega)$.

8.3.3. Feature Characteristics on Albedo

We use the four textures *(gr2, wv2, grd1* and *an4)* to illustrate the feature characteristics of albedo data (three are the same as those used in chapter *6*). Firstly, their albedo images and albedo spectra $A(\omega, \theta)$ in the frequency domain at surface orientation angle of $\varphi = 30°$ are shown in *Figure 8. 14.* Secondly their corresponding polar spectra $\Pi_\beta(\theta)$ on albedo spectra $A(\omega, \theta)$ are shown in *Figure 8. 15*. Finally their polar spectra $\Pi_\beta(\theta)$ on albedo spectra $A(\omega, \theta)$ are shown in *Figure 8. 16*.

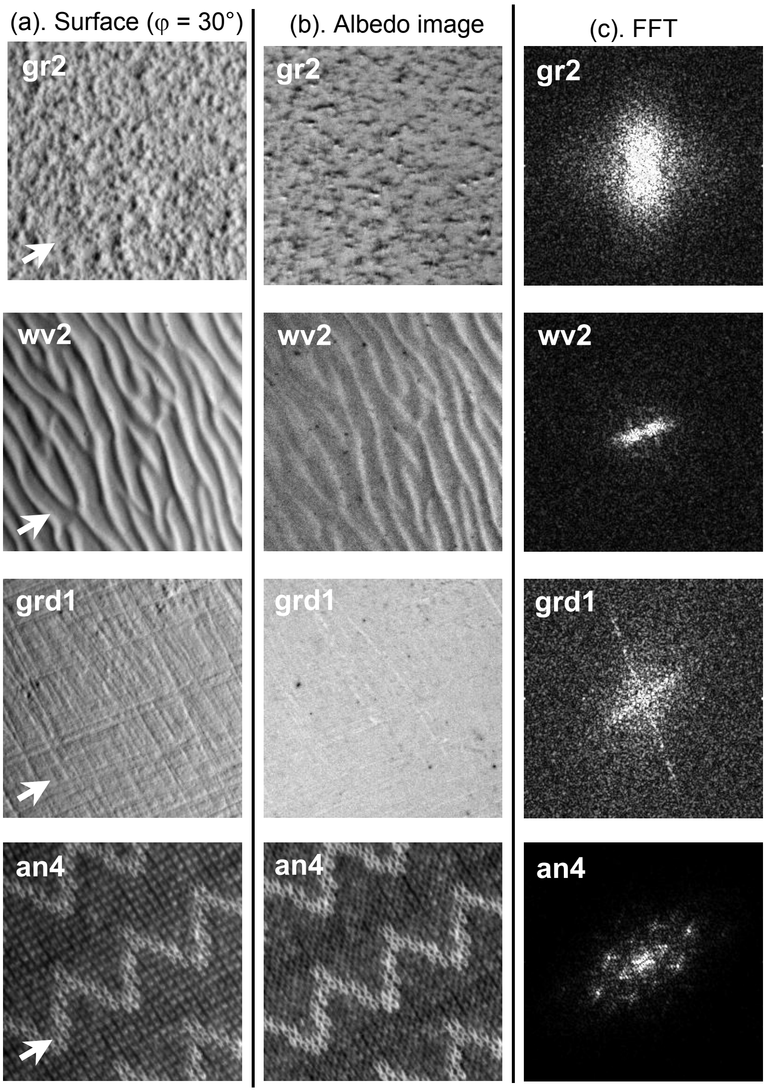

Figure 8. 14 Albedo spectra $A(\omega, \theta)$ for four real textures (gr2, wv2, grd1 and an4). (a). surface at orientation angle of $\varphi = 30°$. (b). their corresponding albedo image $p(x,y)$ obtained by using photometric stereo. (c). their corresponding albedo spectra $A(\omega, \theta)$ in the frequency domain.

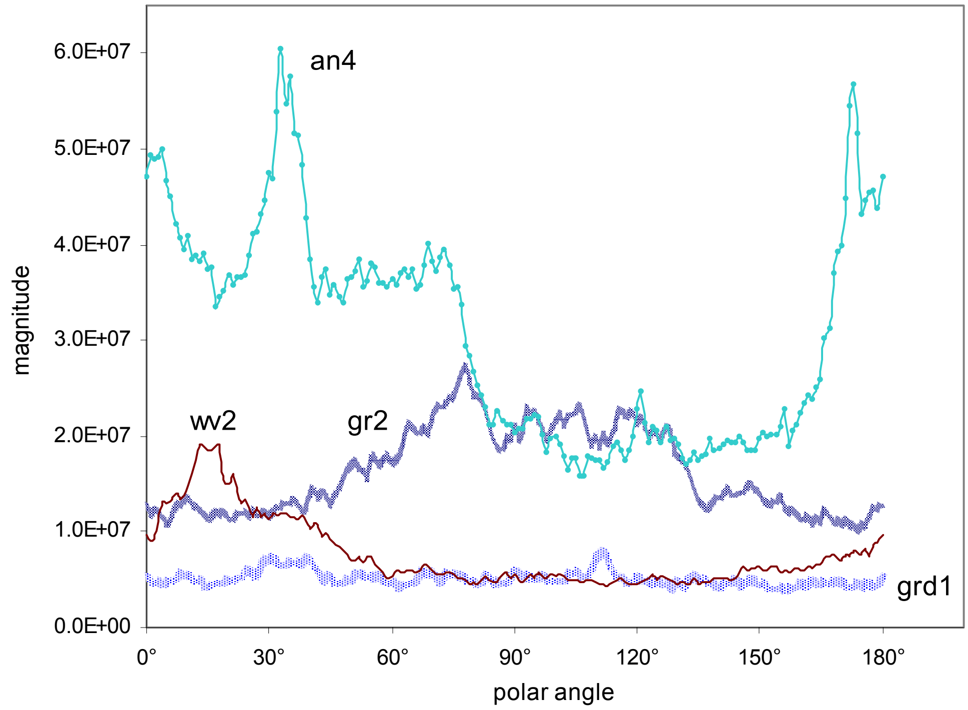

Figure 8. 15 Polar spectrum $\Pi_\beta(\theta)$ on albedo spectra $A(\omega, \theta)$ for four real textrues (gr2, wv2, grd1 and an4) at orientation angle of $\varphi = 30°$.

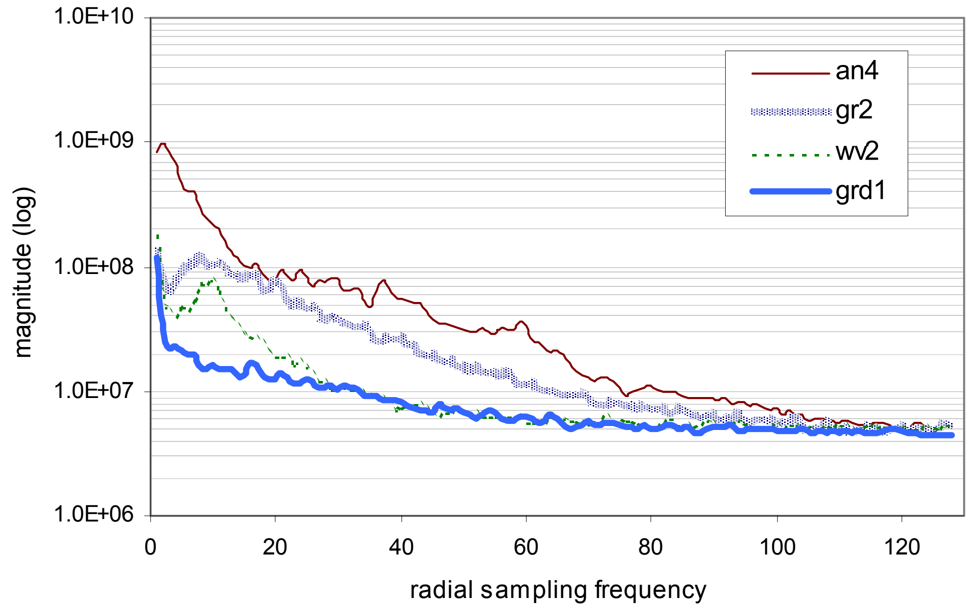

Figure 8. 16 Radial spectrum $\Phi_\beta(\omega)$ on albedo spectra $A(\omega, \theta)$ for four real textrues (gr2, wv2, grd1 and an4) at orientation angle of $\varphi = 30°$.

8.3.4. Albedo Feature Sensitivity to Surface Rotation

Figure 8. 17 shows the albedo images $\rho(x, y)$ at a surface orientation angles of φ = $30°$, $60°$, $90°$ and $120°$ of four textures *(gr2, wv2, grd1 and an4)*, obtained by using photometric stereo. Their corresponding albedo spectra $A(\omega, \theta)$ are shown in *Figure 8. 18*.

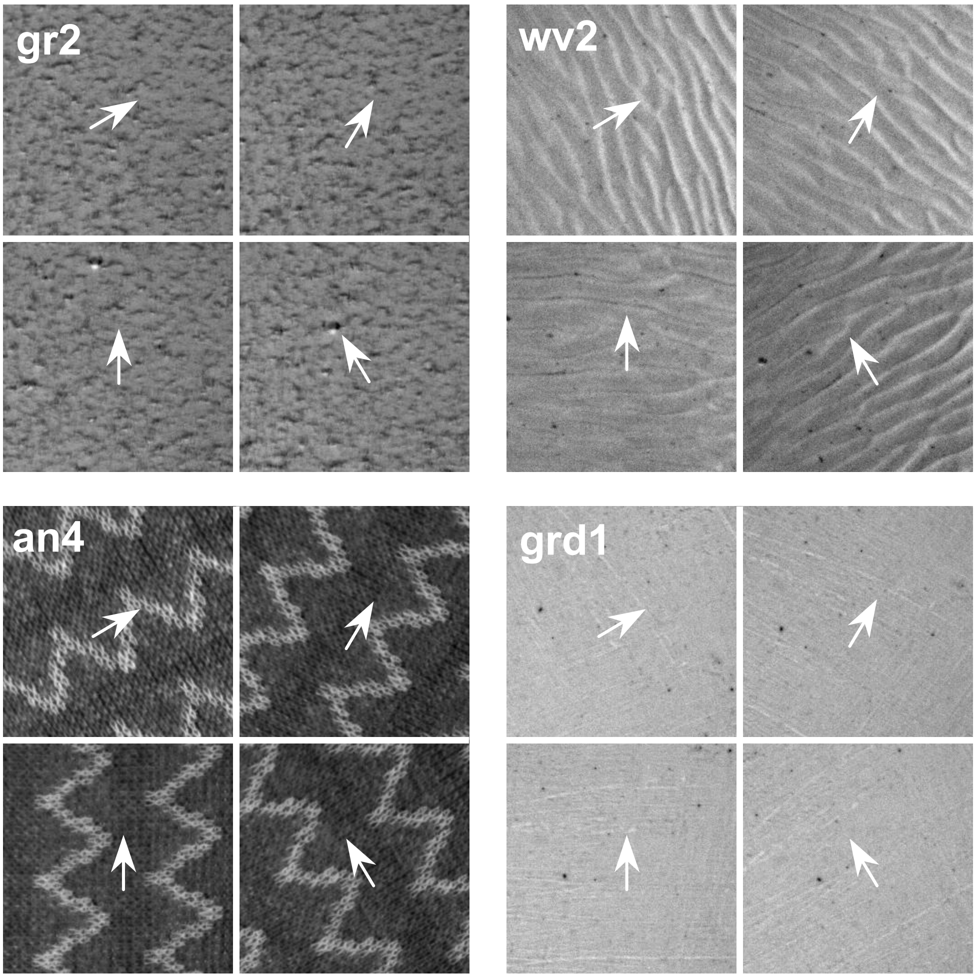

Figure 8. 17 Albedo image $\rho(x,y)$ at surface orientation angles of $\varphi = 30°, 60°, 90°$ and $120°$ for four real textures (gr2, wv2, grd1 and an4). For the purpose of display, they are shown in a montage format where the white arrows indicate the surface rotation directions.

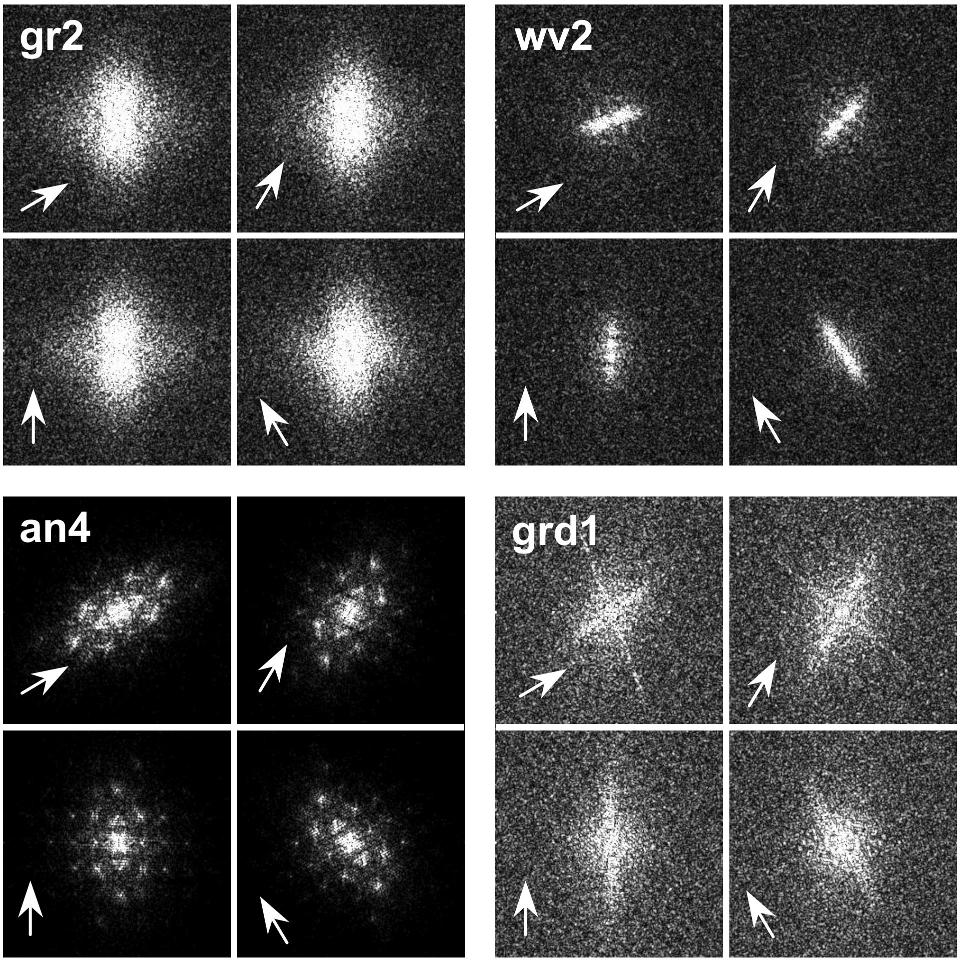

Figure 8. 18 Albedo spectra $A(\omega, \theta)$ at surface orientation angles of φ = 30°, 60°, 90° and 120° for four textures (gr2, wv2, grd1 and an4). For the purpose of display, all four albedo spectra at different surface orientations are displayed in a montage format for each individual texture (the white arrow indicates the surface rotation direcetion).

From these figures, it is clear that albedo data are sensitive to surface rotation in the same manner as gradient spectra $M(\omega, \theta)$ shown before. Therefore, the rotation invariant texture classification scheme previously discussed, using both polar spectra and radial spectra, can be applied.

8.3.5. Developing New Classifiers

- ***Developing three classifiers based on albedo data***

A modified surface rotation invariant texture classification scheme based on albedo data is summarised in *Figure 8. 19*.

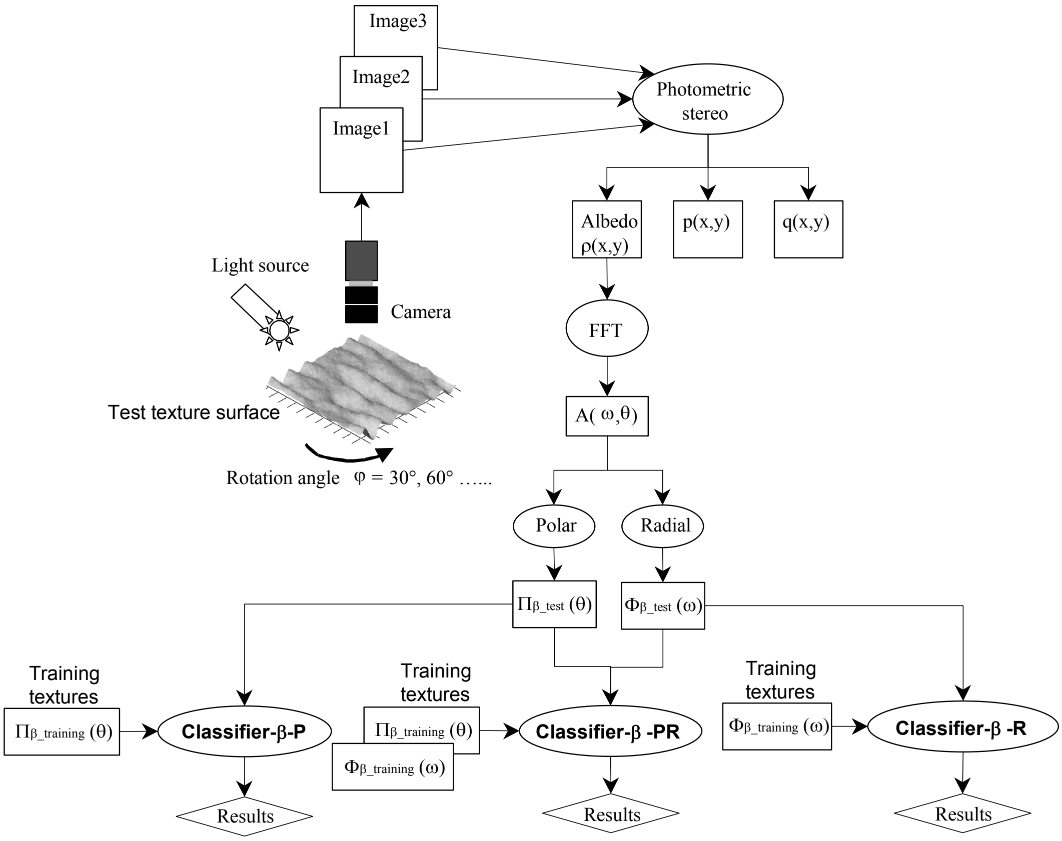

Figure 8. 19 Surface rotation invariant texture classification scheme based on albedo data only. Classifier-β-P is based on the polar spectrum $\Pi_\beta(\theta)$ only; Classifier-β-R is based on the radial spectrum $\Phi_\beta(\omega)$ only; and Classifier-β-PR is based on the combination of the polar spectrum $\Pi_\beta(\theta)$ and radial spectrum $\Phi_\beta(\omega)$ together.

The process is as follows:

1) albedo data $\rho(x,y)$ of the test texture can be directly estimated by using three-image-based photometric stereo.
2) They are then Fourier transformed to give the albedo spectra $A(\omega,\theta)$ and processed to provide the albedo polar spectrum $\Pi_{\beta\_test}(\theta)$ and albedo radial spectrum $\Phi_{\beta\_test}(\omega)$.
3) The polar spectrum $\Pi_{\beta\_test}(\theta)$ of the test texture is compared with the polar spectra $\Pi_{\beta\_training}(\theta)$ obtained from training images using a sum of squared differences metric. As before the task is to minimise the difference metric with

regard to surface orientations. This also provides an estimate of the orientation angle $\varphi_{estimate}$ of the test texture.

4) The radial spectrum $\Phi_{\beta\_test}(\omega)$ is compared with the radial spectra $\Phi_{\beta\_training}(\omega)$ obtained from training images. (This also uses a sum of squared differences metric but it does not need to be calculated over a range of angular displacements, as radial spectra are insensitive to surface orientation.)
5) The total sum of squared errors statistic is calculated from step *3* and *4* and the lowest score provides the classification decision. There are three different kinds of classifier thus allowing a for comparative study.

I. **Classifier-β-P** uses only the albedo polar spectrum $\Pi_{\beta}(\theta)$, and its classification cost function is:

$$SSD_{\beta\_polar} = \sum_{\theta=0°}^{180°} [\,\Pi_{\beta\_test}(\theta+\varphi_{estimate}) - \Pi_{\beta\_training}(\theta)\,]^2 \tag{8. 6}$$

where $\Pi_{\beta\_test}(\theta)$ is the polar spectrum of the albedo spectra $A(\omega,\theta)$ obtained from the *test* texture data set; $\Pi_{\beta\_training}(\theta)$ is the polar spectrum of the albedo spectra obtained from the *training* texture data set; while $\varphi_{estimate}$ is the estimated surface orientation angle; and the resolution of θ is at step $1°$ from $0°$ to $180°$.

II. **Classifier-β-R** is based on the radial spectrum $\Phi_{\beta}(\omega)$ only and its classification cost function is:

$$SSD_{\beta\_radial} = \sum_{\omega=1}^{R} [\,\Phi_{\beta\_test}(\omega) - \Phi_{\beta\_training}(\omega)\,]^2 \tag{8. 7}$$

where $\Phi_{\beta\_test}(\omega)$ is the radial spectrum of the albedo spectra $A(\omega,\theta)$ obtained from the *test* texture data set; $\Phi_{\beta\_training}(\omega)$ is the radial spectrum of the albedo spectra obtained from the *training* texture data set; and R is the high frequency range radius of a circle centred at the origin. For $N\times N$ albedo spectra $A(\omega,\theta)$, R is typically chosen as $N/2$.

III. **Classifier-β-PR** is based on a combination of the polar spectrum $\Pi_{\beta}(\theta)$ and the radial spectrum $\Phi_{\beta}(\omega)$.

$$SSD_{\beta\_polar\&radial} = (SSD^{*}_{\beta\_polar}) + (SSD^{*}_{\beta\_radial}) \tag{8. 8}$$

where $SSD^{*}_{\beta\_polar}$ is the normalised cost function value of SSD_{β_polar} obtained from *Classifier-β-P*; $SSD^{*}_{\beta\_radial;}$ is the normalised cost function value of SSD_{β_radial} obtained from *Classifier-β-R*. We note that the original SSD_{β_polar} and SSD_{β_radial} come from different kinds of feature spaces: polar spectrum and radial spectrum respectively. We have to normalise their values in each feature vector within all of the considered texture classes prior to using the *classifier-β-PR*.

- ***Developing a new classifier based on gradient data for comparison***

In a similar manner to the way in which we developed three albedo based classifiers *(Classifier-β-P, Classifier-β-R and Classifier-β-PR)*, we may define our two exiting classifiers based on gradient data as *Classifier-α-P* (where the feature space comes from the polar spectrum) and *Classifier-α-R* (where the feature space comes from the radial spectrum). In addition, we can extend and develop a new classifier (*Classifier-α-PR)* which combines the polar spectrum and radial spectrum features obtained from gradient data. Note that α indicates that the feature space in a classifier comes from gradient data. On the other hand, β denotes that the feature space in a classifier comes from albedo data. *Figure 8. 20* summarises all three classifiers *(Classifier-α-P, Classifier-α-R and Classifier-α-PR)*.

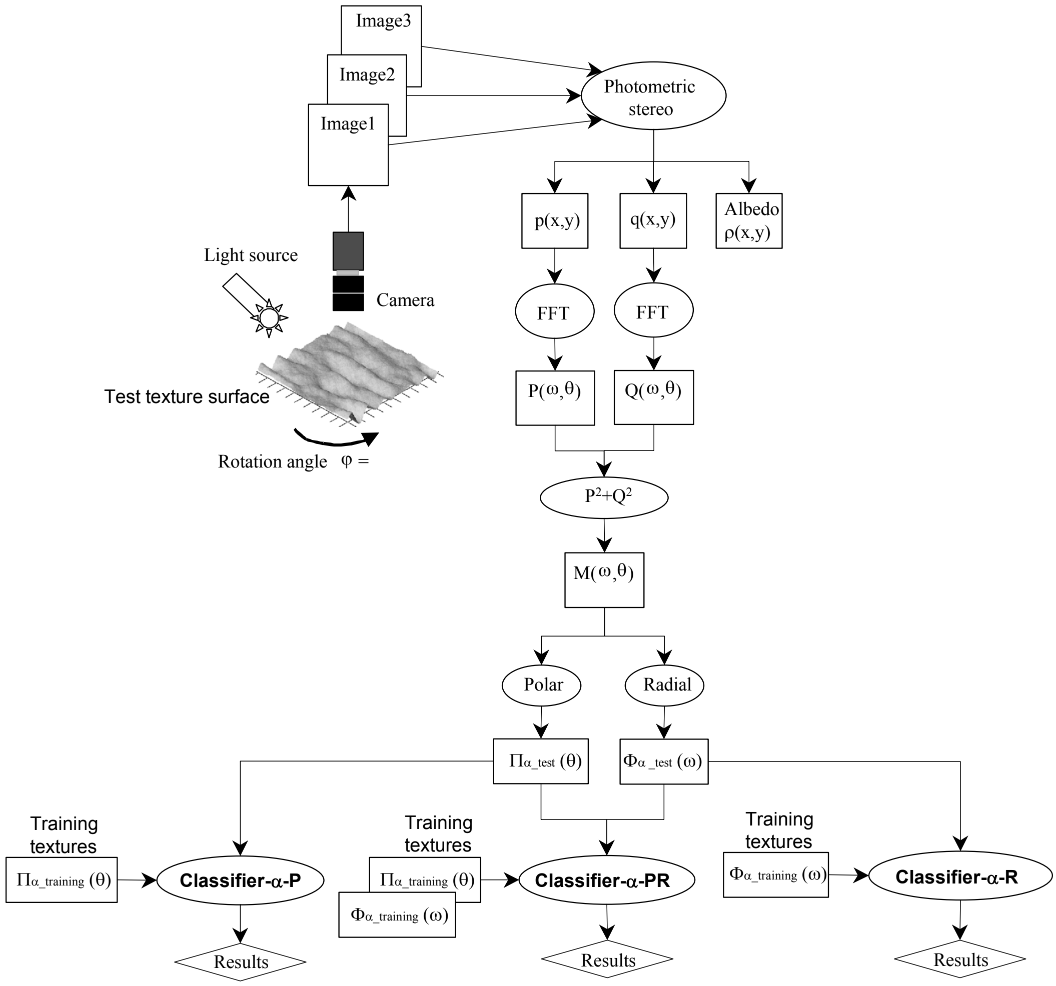

Figure 8. 20 Surface rotation invariant texture classification scheme based on gradient data only. Classifier-α-P is based on the polar spectrum $\Pi_{\alpha}(\theta)$ only; Classifier-α-R is based on the radial spectrum $\Phi_{\alpha}(\omega)$ only; and Classifier-α-PR is based on a combination of the polar spectrum $\Pi_{\alpha}(\theta)$ and the radial spectrum $\Phi_{\alpha}(\omega)$.

The notation of all the designed classifiers in terms of polar spectra and radial spectra on both gradient spectra and albedo spectra is shown in *Table 8. 3*.

Classifier [Feature space]	***Polar spectrum*** $\Pi(\theta)$	***Radial spectrum*** $\Phi(\omega)$	***Polar spectrum*** $\Pi(\theta)$ **&** ***Radial spectrum*** $\Phi(\omega)$
Gradient spectra $M(\omega, \theta)$	Classifier-α-P [$\Pi_{\alpha}(\theta)$]	Classifier-α-R [$\Phi_{\alpha}(\omega)$]	Classifier-α-PR [$\Pi_{\alpha}(\theta)$ & $\Phi_{\alpha}(\omega)$]
Albedo spectra $A(\omega, \theta)$	Classifier-β-P [$\Pi_{\beta}(\theta)$]	Classifier-β-R [$\Phi_{\beta}(\omega)$]	Classifier-β-PR [$\Pi_{\beta}(\theta)$ & $\Phi_{\beta}(\omega)$]

Table 8. 3 Notation of classifiers' design in terms of the polar spectrum and the radial spectrum on both gradient spectra and albedo spectra.

8.3.6. Classification Results on Albedo Data Only

In this section, we will present and discuss the classification results using albedo data only. A comparative study of the classification results for gradient data and albedo data will be given in the next section.

Figure 8. 21 shows classification results for the three albedo-based classifiers derived from *30* real textures. In addition, the overall classification accuracy for the classifiers *(Classifier-β-P, Classifier-β-R and Classifier-β-PR)* is presented in *Table 8. 4*. The *Classifier-β-P* uses only the polar spectrum $\Pi_{\beta}(\theta)$ to achieve an overall classification accuracy of *67.28%* and the *Classifier-β-R* using only the radial spectrum $\Phi_{\beta}(\omega)$ improves this figure to *71.05%*. The *Classifier-β-PR* combining the polar spectrum $\Pi_{\beta}(\theta)$ and radial spectrum $\Phi_{\beta}(\omega)$ actually pushes the classification rate up to *76.54%.*

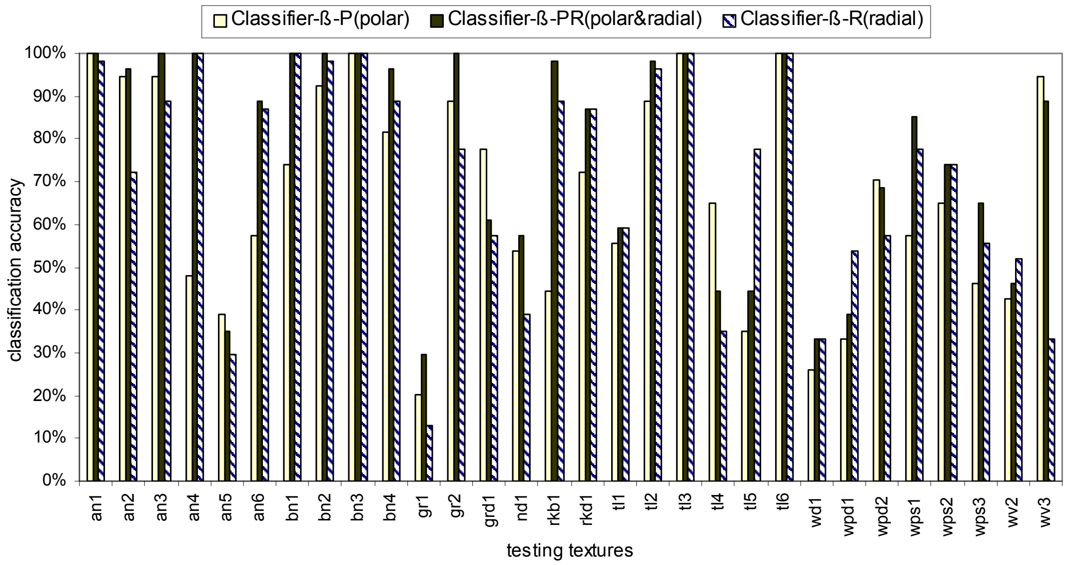

Figure 8. 21 Classification results for 30 real textures based on albedo data only. Note that Classifier-β-P is based on the polar spectrum $\Pi_\beta(\theta)$ only; Classifier-β-R is based on the radial spectrum $\Phi_\beta(\omega)$ only; and Classifier-β-PR is based on a combination of the polar spectrum $\Pi_\beta(\theta)$ and the radial spectrum $\Phi_\beta(\omega)$.

	Polar spectrum $\Pi(\theta)$	***Radial spectrum*** $\Phi(\omega)$	***Polar spectrum*** $\Pi(\theta)$ ***&*** ***Radial spectrum*** $\Phi(\omega)$
Classifier [Feature space]	Classifier-β-P [$\Pi_\beta(\theta)$]	Classifier-β-R [$\Phi_\beta(\omega)$]	Classifier-β-PR [$\Pi_\beta(\theta)$ & $\Phi_\beta(\omega)$]
Overall Classification accuracy	67.28%	71.05%	76.54%

Table 8. 4 Overall classification accuracy for all 30 real textures in three different classifiers (Classifier-β-P, Classifier-β-R and Classifier-β-PR).

We can also see that adding extra feature space, either on the polar spectrum $\Pi_\beta(\theta)$ or on the radial spectrum $\Phi_\beta(\omega)$, improves the overall performance of the classifier on the *30* real textures. In most cases, for each individual texture we note that the classification accuracy obtained from *Classifier-β-PR* is better than those of *Classifier-β-P* and *Classifier-β-R*, apart from a few textures such as *"an5", "grd1", "tl4", "tl5"*.

8.3.7. Comparative Study of Classification Results Between Gradient Data and Albedo Data

We have introduced the new feature generator of albedo data in addition to our existing feature generator of gradient data shown in *Chapter 6*. The classification results from the albedo data have been given and analysed. Now we will discuss the comparative study of classification results for gradient data and albedo data.

- ***The importance of albedo data***

A summary of classification accuracy for texture *"tl3"* is given in *Table 8. 5*. It shows very clear that the successful classification rates obtained from the feature generators of albedo spectra $A(\omega, \theta)$ are *100%* and are much improved compared to those (from *33.33%* to *38.89%*) obtained from the gradient spectrum $M(\omega, \theta)$, whether the feature space is based on the polar spectrum $\Pi(\theta)$, the radial spectrum $\Phi(\omega)$, or the combination of the polar spectrum $\Pi(\theta)$ and the radial spectrum $\Phi(\omega)$.

	Gradient spectra $M(\omega, \theta)$	***Albedo spectra*** $A(\omega, \theta)$
Polar spectrum $\Pi(\theta)$	33.33%	100% ↑
Radial spectrum $\Phi(\omega)$	38.89%	100% ↑
Polar spectrum $\Pi(\theta)$ ***&*** ***Radial spectrum*** $\Phi(\omega)$	33.33%	100% ↑

Table 8. 5 Classification accuracy for texture "tl3" for gradient feature space $M(\omega, \theta)$ and albedo feature space $A(\omega, \theta)$.

We may draw the conclusion that albedo can be an important feature in our classification schemes.

- ***Classification results only based on gradient data for all 30 real textures***

Before we consider the comparative study on the classification results for gradient data and albedo data, we firstly extend our existing surface rotation invariant texture classification scheme on gradient data to a full range of classifiers *(Classifier-α-P, Classifier-α-R and Classifier-α-PR in Figure 8. 20)* in the same manner as was we have done with the albedo data *(Classifier-β-P, Classifier-β-R and Classifier-β-PR in Figure 8. 19)*.

The classification results for *30* real textures based on gradient data are shown in *Figure 8. 22* and *Table 8. 6*.

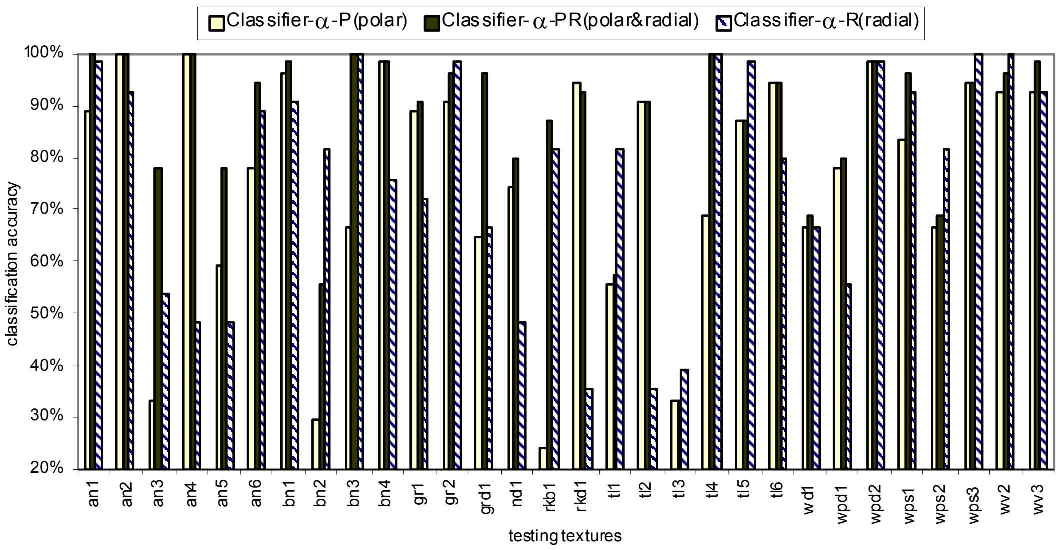

Figure 8. 22 Classification results for 30 real textures based on gradient data only. Note that Classifier-α-P is based on the polar spectrum $\Pi_\alpha(\theta)$ only; Classifier-α-R is based on the radial spectrum $\Phi_\alpha(\omega)$ only; and Classifier-α-PR is based on a combination of the polar spectrum $\Pi_\alpha(\theta)$ and the radial spectrum $\Phi_\alpha(\omega)$.

Classifier	Classifier based on gradient spectra $M(\omega, \theta)$		
	Classifier-α-P [$\Pi_\alpha(\theta)$]	*Classifier-α-R* [$\Phi_\alpha(\omega)$]	*Classifier-α-PR* [$\Pi_\alpha(\theta)$ & $\Phi_\alpha(\omega)$]
Overall 30 real textures	**76.30%**	**76.67%**	**86.91%** ↑↑

Table 8. 6 Comparison of classification accuracy for three different classifiers (Classifier-α-P, Classifier-α-R and Classifier-α-PR) on gradient spectra $M(\omega, \theta)$, for 30 real textures and some selected texture samples.

- ***Comparative study of classification results between gradient data and albedo data***

Now it is time to give the comparative study of classification results for the gradient data and albedo data. In *Figure 8. 23*, we only give the results for two of the classifiers *(Classifier-α-PR and Classifier-β-PR)* based on gradient data and albedo data respectively. On the other hand, *Table 8. 7* provides the comparative classification results for all the six classifiers *(Classifier-α-P, Classifier-α-R, Classifier-α-PR, Classifier-β-P, Classifier-β-R and Classifier-β-PR)*.

We note:

1) That the classification accuracy based on gradient spectra $M(\omega, \theta)$ is better than that obtained from albedo spectra $A(\omega, \theta)$, whether the feature space used is the polar spectrum $\Pi(\theta)$, radial spectrum $\Phi(\omega)$ or their combination.
2) The classification results derived from the combination of feature spaces (the polar spectrum $\Pi(\theta)$ and the radial spectrum $\Phi(\omega)$) are better than those derived from the individual feature spaces alone.
3) We may integrate the feature generators of gradient spectra $M(\omega, \theta)$ and albedo spectra $A(\omega, \theta)$ together to provide more discriminative ability.

	Polar spectrum $\Pi(\theta)$	***Radial spectrum*** $\Phi(\omega)$	***Polar spectrum*** $\Pi(\theta)$ ***& Radial spectrum*** $\Phi(\omega)$
Gradient spectra $M(\omega, \theta)$	76.30% [Classifier-α-P]	76.67% [Classifier-α-R]	86.91% [Classifier-α-PR]
Albedo spectra $A(\omega, \theta)$	67.28% [Classifier-β-P]	71.05% [Classifier-β-R]	76.54% [Classifier-β-PR]

Table 8. 7 A full comparative study of overall classification results for 30 real textures for gradient data features and albedo data features.

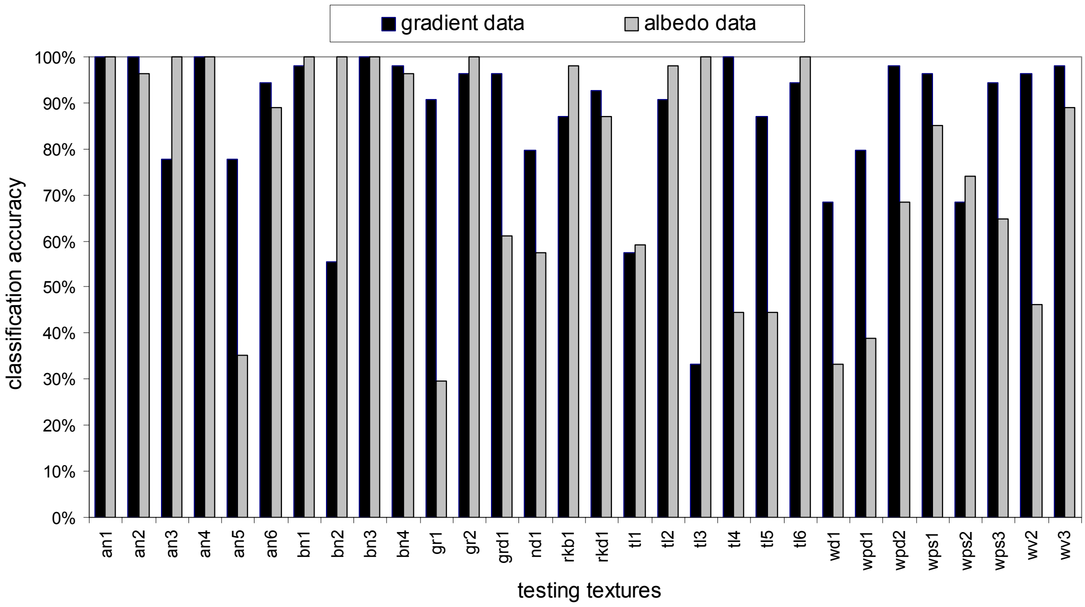

Figure 8. 23 Comparison of classification results for 30 real textures for Classifier-α-PR (obtained from gradient data with the combination of the polar spectrum and the radial spectrum) and Classifier-β-PR (obtained from albedo data with the combination of the polar spectrum and the radial spectrum).

8.4. An Improved Surface Rotation Invariant Classification Scheme by Combining Feature Spaces and Feature Generators

8.4.1. Summary of Classification Scheme

We have already noted that radial spectra can provide very useful features for classification, and albedo information can be important as a feature generator. Therefore, we integrate those two feature space (*polar spectra* and *radial spectra*) and two feature generators (*gradient data* and *albedo data*) in our improved surface rotation invariant classification scheme, illustrated in *Figure 8. 24*.

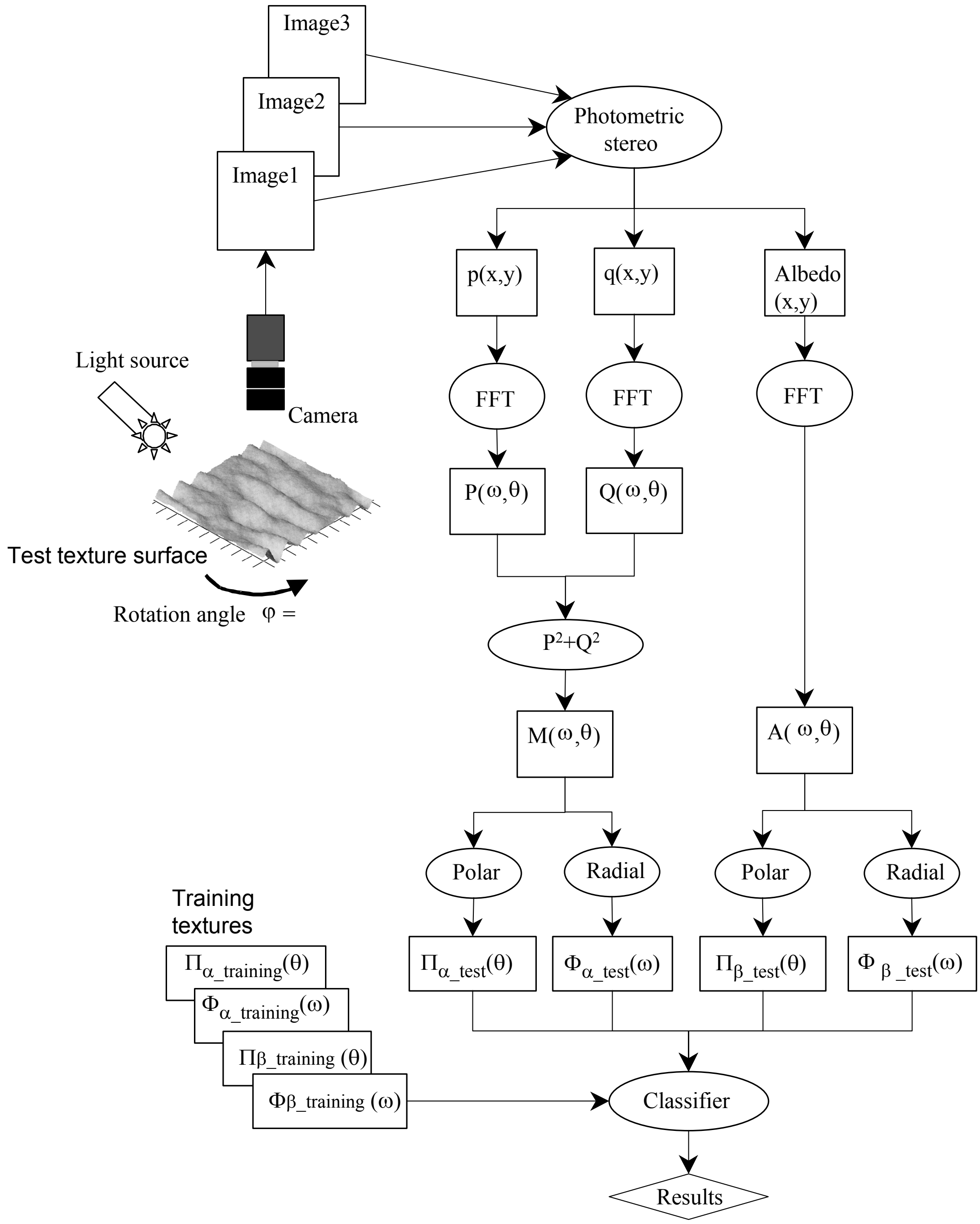

Figure 8. 24 An improved surface rotation invariant texture classification scheme based on both gradient data $M(\omega, \theta)$ and albedo data $A(\omega, \theta)$. Note that feature spaces are polar spectra $\Pi(\theta)$ and radial spectra $\Phi(\omega)$.

The summary of the process is as follows:

1) Gradient data $M(\omega, \theta)$ and albedo data $A(\omega, \theta)$ for each test surface at certain orientation angle is estimated by using photometric stereo algorithm.

2) Gradient data $M(\omega, \theta)$ then provides the gradient polar spectrum $\Pi_{\alpha\_test}(\theta)$ and the gradient radial spectrum $\Phi_{\alpha\_test}(\omega)$. Albedo data $A(\omega, \theta)$ then provides the albedo polar spectrum $\Pi_{\beta\_test}(\theta)$ and the albedo radial spectrum $\Phi_{\beta\_test}(\omega)$.
3) Both the gradient polar spectrum $\Pi_{\alpha\_test}(\theta)$ and albedo polar spectrum $\Pi_{\beta\_test}(\theta)$ of the test texture is compared with the polar spectrum obtained from the training image to produce the difference metric in the same way as described before. At the same stage, the surface orientation of the test texture can also be estimated.
4) While both the gradient radial spectrum $\Phi_{\alpha\_test}(\omega)$ and the albedo radial spectrum $\Phi_{\beta\_test}(\omega)$ are compared with the radial spectrum obtained from the training textures, the difference metric is also calculated.
5) The total sum of squared errors statistic is calculated from steps *3* and *4*, and the best matching provides a classification decision.

8.4.2. Classification Results

In order to compare the classification results, we show our new improved classification results with other two classifiers' results (*Classifier-α-PR* and *Classifier-β-PR* presented in *Figure 8. 23* and *Table 8. 7*) together. *Figure 8. 25* shows the comparative classification results per texture for these three versions of the classifier by using polar and radial spectra. The "*albedo*" classifier used only the albedo radial and polar spectra to achieve a classification accuracy of *76.54%*, using gradient data only ("*gradient*") improved this figure to *86.91%*, while combining gradient and albedo data pushed the classification rate up to *90.56%* (*"gradient & albedo"*). It also shows that integration of the feature generators of gradient and albedo together provides more discriminative ability and comprehensive information for the classifier.

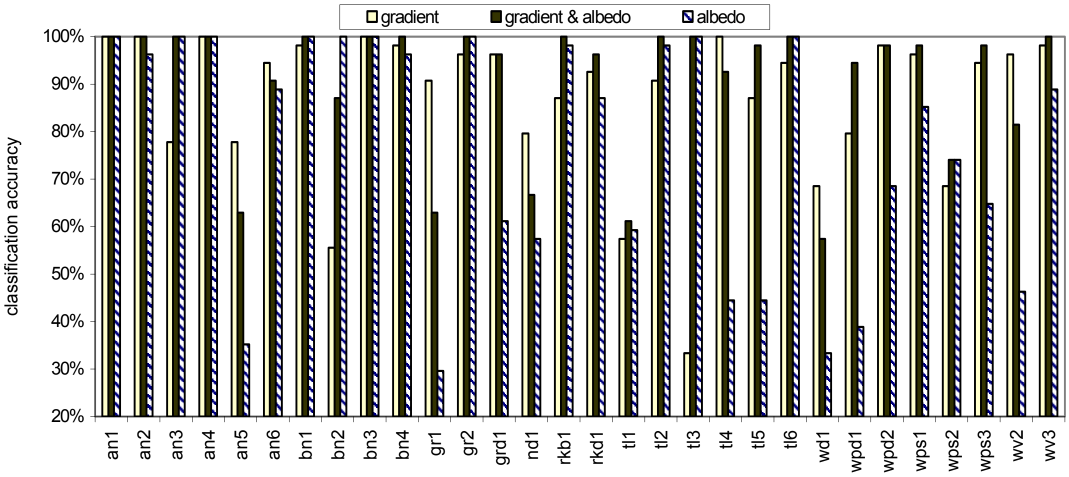

Figure 8. 25 Classification results for 30 real textures between our new improved classifier ("gradient & albedo"), and Classifier-α-PR (based on "gradient" data) and Classifier-β-PR (based on "albedo" data).

8.5. Summary

In this chapter, we introduce a new classification feature space, *radial spectrum* in addition to *polar spectrum* and a new feature generator, *albedo spectra* in addition to *gradient spectra* in order to provide additional information on surface texture properties. Furthermore, the comparative classification results show that the integration of more feature spaces and more feature generators provides more discriminative ability for the classifier, finally our new improved classification scheme achieves the best result with the classification accuracy of *90.56%* for all *30* real textures.